IJP

Check for updates

ORIGINAL PAPER

Temporal variability of galactic cosmic ray intensity and its dependence on various solar parameters observed during solar cycles 23 and 24

P Srivastava* and **A K Singh**

Department of Physics, University of Lucknow, Lucknow 226007, India

Abstract: In this study, we have investigated the solar modulation of galactic cosmic rays (GCRs) during solar cycles 23 and 24. The periods comprise two epochs of negative and positive polarities of the heliospheric magnetic field from the Sun's North Polar Region. We have used concurrent solar and interplanetary magnetic field data, the tilt angle of the heliospheric current sheet (HCS), and the cosmic ray data as the inputs to obtain the required results. During these two cycles, we have investigated the relationship between simultaneous fluctuations in cosmic ray intensity and solar/interplanetary parameters as obtained by some previous researchers. We have noticed several unusual aspects in cosmic ray modulation, including a high GCRs intensity in SC24 compared with the previous solar cycle. The Pearson's correlation of GCRs intensity with considered solar parameters is $r_{\text{GCRs vs SSN}}$ (-0.79) in SC 23 and (-0.91) in SC 24, $r_{\text{GCRs vs F10.7}}$ (-0.88) in SC23 and (-0.87) in SC 24. The relationships of GCRs intensity with interplanetary parameters also are strongly anticorrelated except for IMF (Bz) in solar cycle 24 and solar wind speed in both cycles. The Pearson's correlation of GCRs intensity and interplanetary parameters is $r_{\text{GCRs vs IMF}}$ (-0.73) in SC23 and (-0.46) in SC 24, $r_{\text{GCRs vs HCS}}$ (-0.77) in SC 23 and (-0.87) in SC 24. We also have used time lag and Spearman's correlation coefficient to determine the monotonicity of GCRs intensity and solar/interplanetary characteristics. Thus, we have concluded that the intensity of GCRs has inverse relationships and has been significantly impacted by solar and interplanetary parameters with time lag over both solar cycles 23 and 24.

Keywords: Solar activity; Solar cycle; Sunspot number; Interplanetary magnetic field; Galactic cosmic rays

1. Introduction

GCRs near the Earth were strongly modulated due to the solar magnetic activity [1–3]. The role of galactic cosmic ray modulation has essential aspects because it can reveal subtle features of energetic charged particle transport in the tangled fields that pervade the heliosphere, as well as to learn about the physics of the processes operating into the Sun [4, 5]. The long-term GCRs modulation cycle has 11-year variations with the solar cycle, and the drift of the GCRs in the heliosphere depends on the polarity of the solar magnetic field. The solar magnetic field reversed at each maximum of solar activity [6, 7]. The solar polarity (A) is positive when the field points away from the Sun in the northern hemisphere and negative when it points away from the Sun in the southern hemisphere. The A > 0 epoch

denotes a positive polarity field, whereas the A < 0 epoch denotes a negative field [8]. The response of GCRs intensity to fluctuations in solar activity during the A < 0 epochs differs from that observed in a long-term record of cosmic ray intensity during the A > 0 solar polarity epochs [9]. GCRs modulation depends on the structure and strength of the heliospheric magnetic field, and the proxies suitable for evaluating magnetic are solar wind characteristics and sunspot numbers [2].

During the solar minimum, it has been found that GCRs intensity increases, and during the solar maximum, it decreases [10]. Forbush [11] discovered that the intensity of GCRs, as seen from the Earth and in the Earth's orbit, has an estimated 11-year fluctuation that is anticorrelated with solar activity, with some time lag. Many research groups have attempted to express this long-term change in GCRs intensity using relevant solar indices and geophysical factors [12]. The manipulation of GCRs in the heliosphere using theoretical and empirical techniques is successful and quickly progressing [13]. The link of long-

*Corresponding author, E-mail: rajat.priyank44@gmail.com

term cosmic ray changes with distinct solar-heliospheric parameters and current empirical models of cosmic ray intensity are given special consideration in cosmic ray modulation [14].

In this study, we have investigated the temporal variations of GCRs and their dependence on solar parameters such as sunspot numbers, F10.7 cm index, and solar flux as well as interplanetary parameters, viz. interplanetary magnetic field (Bz), heliospheric current sheet, and solar wind speed during the last two solar cycles 23 and 24. As the last solar cycle 24 was the weakest cycle comparatively [15], greater levels of GCRs intensity were observed. This paper is organized into five sections. Section 1 provides a brief overview of GCRs and their temporal fluctuations with solar and interplanetary factors. Data analysis and adopted methodology are presented in Sect. 2, while Sect. 3 addresses the results and discussion part in detail. Time-lag correlative and Spearman's correlation for monotonicity and peak correlation are covered in Sect. 4, and finally, conclusions are given in Sect. 5. In this study, we have found that during Solar Cycles 23 and 24, the intensity of Galactic Cosmic Rays (GCRs) has an inverse connection with solar and interplanetary parameters and is considerably influenced by them. Furthermore, there is frequently a temporal lag between changes in solar and interplanetary parameters and their influence on GCRs intensity.

## 2. Data sources, analysis, and methodology

For this study, monthly averaged data of sunspot numbers (SSN) have been taken from the World Data Center, Silso, https://wwwbis.sidc.be/silso/datafiles. The Oulu neutron monitor data observed during 1996–2019 have been used to examine the long-term variation in galactic cosmic ray intensity. The time series of monthly averaged cosmic ray intensity data observed during solar cycles 23 and 24 have been considered for the temporal variation. The intensity of the F10.7 index, interplanetary magnetic field (IMF, B_z), and solar wind speed data have been obtained from the OMNI database (https://omniweb.gsfc.nasa.gov/form/dx1.html). The Wilcox Solar Observatory database, http://wso.stanford.edu/Tilts.html, has been used to acquire data on the tilt of the heliospheric current sheet (HCS) using the classic PFSS model [16].

Figure 1 depicts the time profile variations of GCRs intensity and various solar parameters used in this study. (The extended minimum is shown with the dashed line.) All the considered solar parameters and GCRs intensity have been smoothed by the adjacent-averaging method with a window size of 21 months. Adjacent-averaging smoothing is a method of smoothing data by taking the average of a set of adjacent values. This can help reduce noise or fluctuations in a dataset, making it simpler to spot patterns or trends. Smoothing is often applied to time series data to identify trends over time. The number of adjacent data points used for averaging can be changed to obtain the desired level of smoothing. Pearson's correlation and least-squares fitting are used to determine the link between galactic cosmic ray intensity. Pearson's correlation is a statistical measure of a two-variable linear relationship. It runs from -1 to 1 and represents the relationship's intensity and direction. A value of 1 denotes a perfect positive linear relationship, -1 denotes a perfect negative linear relationship, and 0 denotes no linear relationship. Pearson's correlation is a regularly used measure of the relationship between variables in regression analysis. It does, however, presume that the variables' relationships are linear and that the variables are regularly distributed. Spearman's rank correlation coefficient $[\rho]$ and time-lag correlative analysis were used to find the peak correlation and lags in GCRs modulation to solar and interplanetary parameters. Spearman's rank correlation coefficient is a statistical measure used to evaluate the monotony of two variables. It has a value between -1 and 1, with -1 being a perfect negative monotonic relationship, 1 representing a perfect positive monotonic relationship, and 0 representing no monotonic relationship. It is computed by first converting the original data to ranked data and then computing the Pearson correlation coefficient between the ranked data. Spearman's rank correlation coefficient is helpful for non-normally distributed data or when the relationship between variables is nonlinear. Time-lag correlative analysis is a technique used in time series analysis to analyze the association between two variables at distinct periods, often known as lags. The goal of this study is to determine if changes in one variable are related to changes in another variable after a particular period. The study entails computing the correlation coefficient between two time series with varying time delays. Positive correlations at a positive time lag conclude that changes in the first variable cause changes in the second variable.

In contrast, positive correlations at a negative time lag indicate that changes in the second variable cause changes in the first variable. In order to plot the fluctuations of GCRs intensity versus solar/interplanetary parameters, the normalized value of inverse GCRs intensity has been used, which has represented the normalized decrease relative to the maximum intensity, and the solar and interplanetary parameters also have been normalized. Table 1 lists the comparison of Pearson's correlation coefficient (r) and Spearman's correlation rank $[\rho]$ for solar cycles 23 and 24.

Fig. 1 Time series variations of GCRs and considered solar parameters for the period 1996–2019. The vertical dashed line shows the extended minima of solar activity, and the dashed line with the horizontal axis shows the adjacent-averaging smoothing of variables for the window size of 21 months
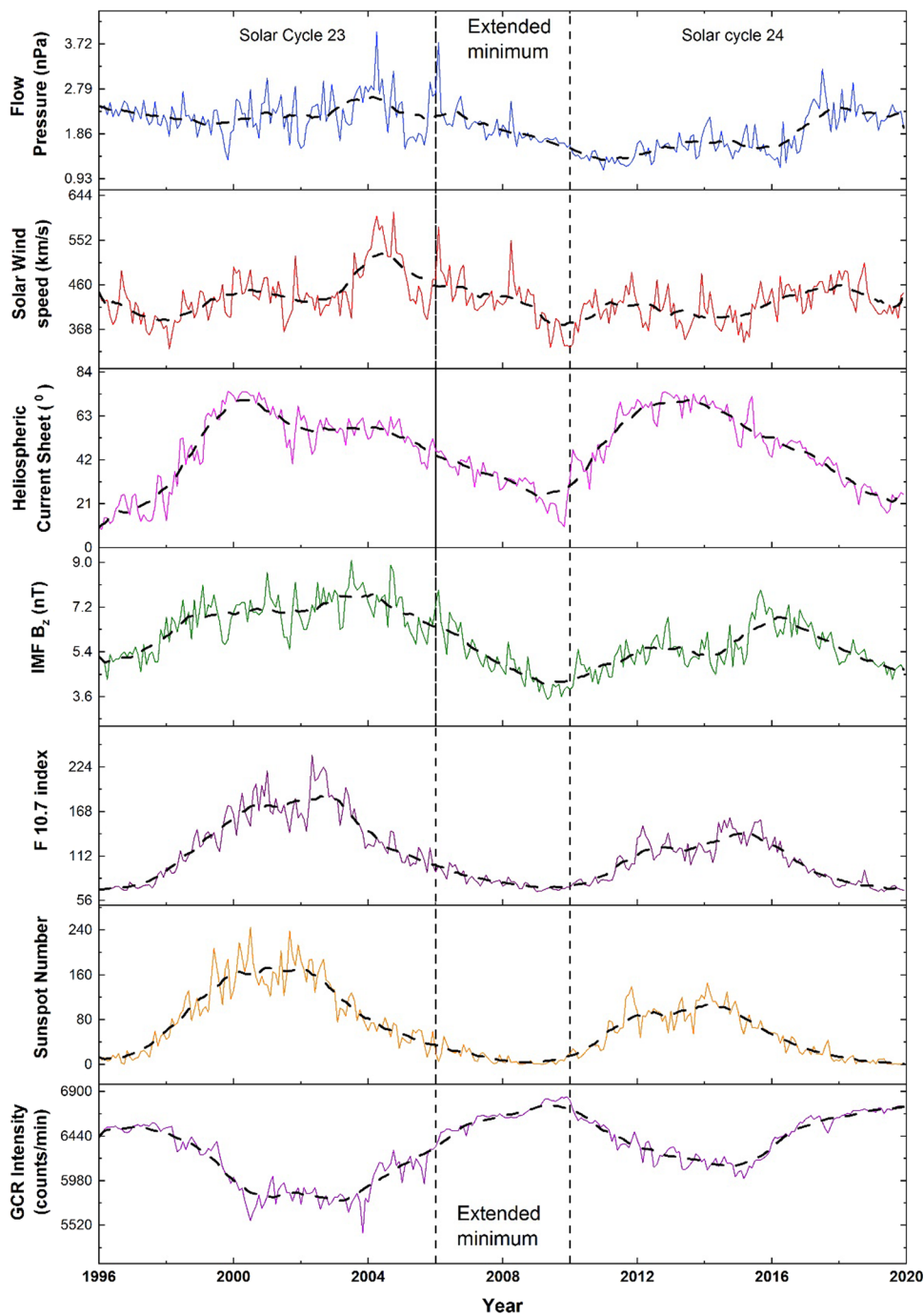
3. Variations in GCRs intensity, solar, and interplanetary parameters

It is very critical to investigate the solar dynamo and transients, which affect the structure of the heliosphere and the modulation of cosmic rays through the degree of solar activity, HCS, solar wind speed, and turbulence intensity of the interplanetary magnetic field (IMF, Bz) [17]. The solar wind, propelled by the solar dynamo, generates a magnetic bubble known as the heliosphere surrounding the solar system. This heliosphere works as a shield, deflecting and modulating incoming cosmic rays from the interstellar medium (the space between stars). The heliosphere extends when the solar wind is more substantial, such as during periods of high solar activity and lowering the input of cosmic rays. During periods of low solar activity, on the other hand, the heliosphere decreases, enabling more cosmic rays to reach the solar system. The magnetic field carried by the solar wind influences the path of cosmic rays. Cosmic rays are charged particles that interact with

Table 1 Time lags, the corresponding cross-correlation coefficient [ρ], and Pearson's correlation coefficient (r) between NM GCRs count and solar/interplanetary parameters for solar cycles 23–24

| Indices	Solar cycle 23			Solar cycle 24		
	r	ρ	Lag (months)	r	ρ	Lag (months)
Sunspot number (SSN)	− 0.79	− 0.84	− 4	− 0.91	− 0.87	− 2
F10.7 index	− 0.88	− 0.89	− 3	− 0.87	− 0.87	0
Interplanetary magnetic field (Bz)	− 0.73	− 0.73	0	− 0.46	− 0.54	9
Heliospheric current sheet tilt angle (°)	− 0.77	− 0.78	− 1	− 0.87	− 0.87	0

the solar magnetic field as they pass through the heliosphere, causing deflection and scattering. This mechanism has the potential to affect the distribution and energy spectrum of cosmic rays measured close to Earth. The sunspot numbers (SSN), the oldest explicitly measured solar activity parameter on the photosphere and chromosphere, are a highly valuable solar activity indicator. The 10.7 cm solar radio flux is the other parameter used to measure the solar activity in the upper and lower chromosphere. Over a long temporal scale, both of these solar activity indicators are anticorrelated to galactic cosmic ray intensity. Thus, these solar parameters (SSN, F10.7) and interplanetary characteristics (SWS, IMF, HCS) as well as the neutron monitor count rate (Oulu neutron monitor with cutoff stiffness Rc = 0.85 GV, 65.05°N, 25.47°E) have been used to investigate the relationship between the GCRs intensity and solar/interplanetary parameters. "GV" in the context of neutron monitors stands for "Geomagnetic Cutoff Rigidity" or "Geomagnetic Rigidity Cutoff." The geomagnetic cutoff rigidity (GV) is a measure of the lowest stiffness (momentum per unit charge) required for a charged particle to reach the Earth's surface at a certain point. In other words, it indicates the bare minimum of energy required for a cosmic ray particle to cross through the geomagnetic field and reach the Earth's atmosphere and surface. Neutron monitors detect cosmic ray particles with energy more significant than the local geomagnetic cutoff stiffness. As a result, the value of GV is a crucial parameter for evaluating neutron monitor data since it helps researchers understand which energy of cosmic rays is being detected at a certain point on Earth. The magnitude of the GV depends on the latitude and altitude of the observation point, as well as the strength of the local geomagnetic field. Figure 1 shows the temporal fluctuation of the solar and interplanetary parameters with GCRs intensity. The dashed vertical line depicted the extended minimum period at the end of solar cycle 23 and the beginning of solar cycle 24. A temporal lag has been observed as the influence of solar and interplanetary factors on the GCRs intensity takes longer.

Figure 2 presents a monthly averaged, normalized, and smoothed (adjacent averaging using a window size of 21 months) graph of the inverse of GCRs intensity, SSN, F10.7 index, IMF (Bz), HCS, and SWS to compare the fluctuation of GCRs intensity with the solar and interplanetary parameters. The inverse of GCRs intensity transformed the plot in the same way that the solar cycle's temporal fluctuation occurs. The HCS divides the heliosphere's two oppositely oriented magnetic polarity hemispheres [6]. The tilt angle of the HCS varies with solar activity and has a period of around 11 years. An inclined current sheet has a substantial impact on the global heliospheric field and cosmic ray particle drift movements [18]. Thus, from the perspective of particle drifts, the tilt of the HCS has become a primary indication of solar activity, and the wavy HCS is one of the most significant physical effects in the modeling of cosmic ray modulation [19]. The HCS shows a continual change with the ascending and descending phases and a maximum of solar cycles, as well as the polarity reversal at the end of solar cycle 23 (Dec 2008). IMF (Bz) was likewise larger in solar cycle 23 than in solar cycle 24, and the temporal fluctuation of IMF (Bz) and the inverse of GCRs intensity are the same as it was with the solar parameters (SSN, F10.7 index), while the solar wind speed has shown a higher value with a higher value of the inverse of GCRs intensity and vice versa.

### 3.1. GCRs intensity vs sunspot numbers, F10.7 cm index

Figure 3 shows the monthly mean GCRs intensity plotted against the monthly mean values of sunspot numbers for solar cycles 23 and 24. From Fig. 3, it can be inferred that as the solar cycle increases, there is a downfall in the GCRs intensity, as solar transients provide a shielding effect and counter the expansion of GCRs in the heliosphere. In solar cycle 23, the mean SSN was ∼ 78.76, and GCRs intensity was found to be ∼ 6224, while in solar cycle 24, the mean SSN was ∼ 49.47, and GCRs intensity was found to be ∼ 6464.

Fig. 2 Temporal variations of normalized and smoothed values of the monthly mean (GCRs intensity)$^{-1}$, sunspot numbers, F10.7 index, interplanetary magnetic field (B$_z$), heliospheric current sheet (deg), solar wind speed (km s^{-1}). The vertical black and red dotted line shows that during an extended minimum, there is an increment in the normalized solar and interplanetary variables but a decrement in the normalized (GCRs intensity)$^{-1}$
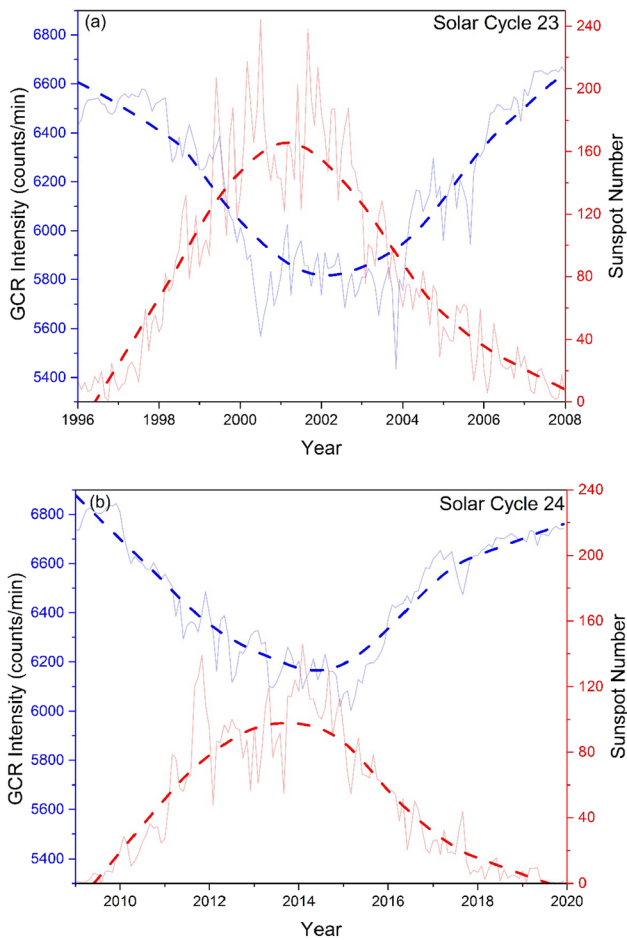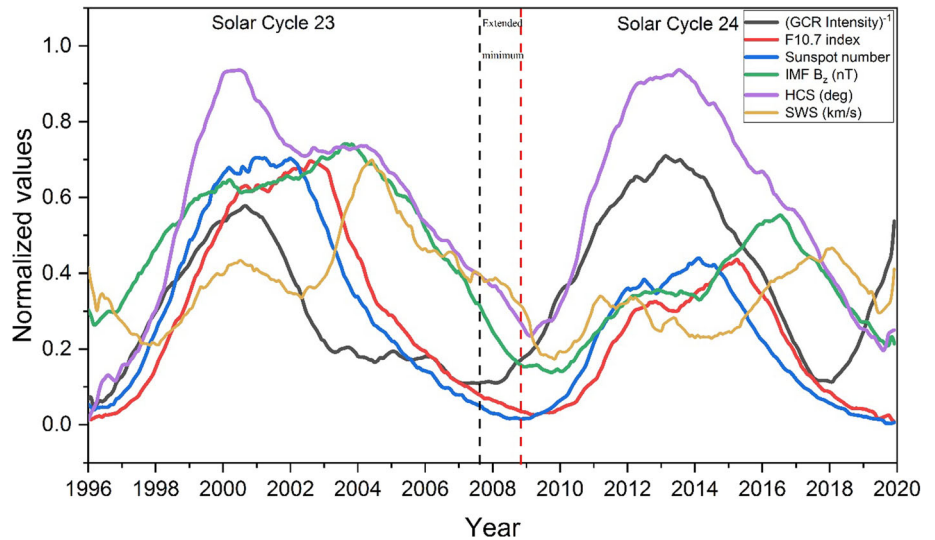
Fig. 3 Monthly mean GCRs intensity and monthly mean SSN trend and distribution for solar cycles 23 and 24. The blue dashed curve shows a smoothing curve for SSN, and the red dashed curve shows a smoothed curve of GCRs intensity

Solar activity has long been recognized to alter the strength as well as the energy spectrum of GCRs [20, 21].
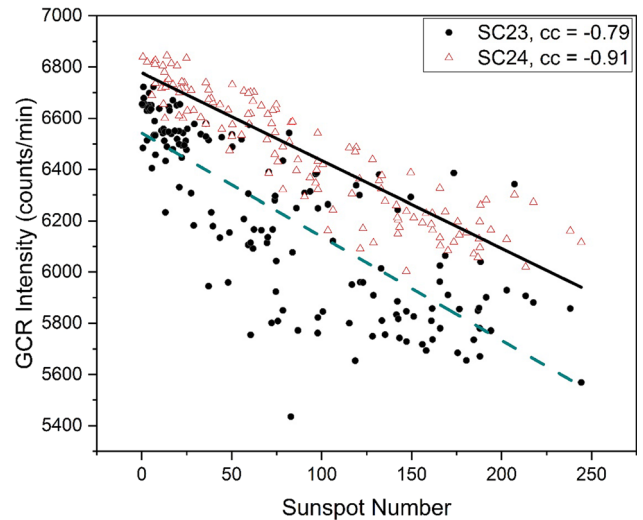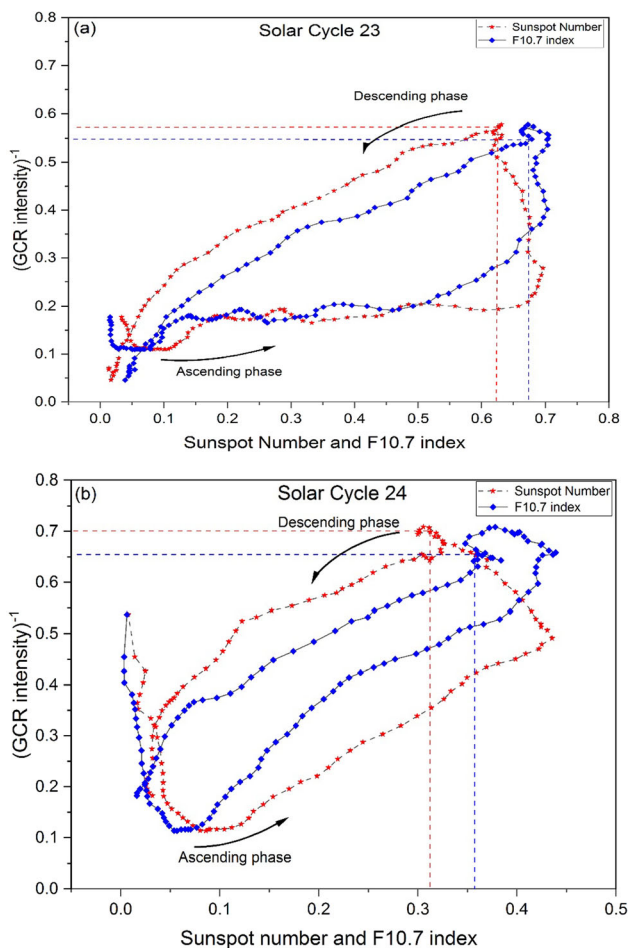
Fig. 4 Scattered plot between monthly mean GCRs intensity and SSN for solar cycles 23 and 24. The black and blue dashed line shows a linear regression of GCRs and SSN

Many studies have noted the anticorrelation and anisotropies in the solar modulation of cosmic rays, as well as differences in time lag for odd and even cycles [22, 23]. To explain the enhancement to the dependence of GCRs intensity on sunspot numbers, we have used Pearson's correlation approach. We have observed that the GCRs intensity and sunspot numbers are anticorrelated, and it confirms that during the solar minimum, GCRs activity increases. Figure 4 shows a scattered plot between GCRs intensity and sunspot numbers. However, it revealed that for both cycles 23 and 24, GCRs intensity and SSNs have shown strong anticorrelation with each other. Pearson's correlation and least square fitting are used to determine the relationship between these variables. Pearson's correlation coefficient (r) for solar cycle 23 was observed at − 0.79,

and for solar cycle 24, it was − 0.91. Thus, as expected from Forbush's initial study, there is an inverse relationship between cosmic ray intensity and solar activity as measured by sunspot counts.
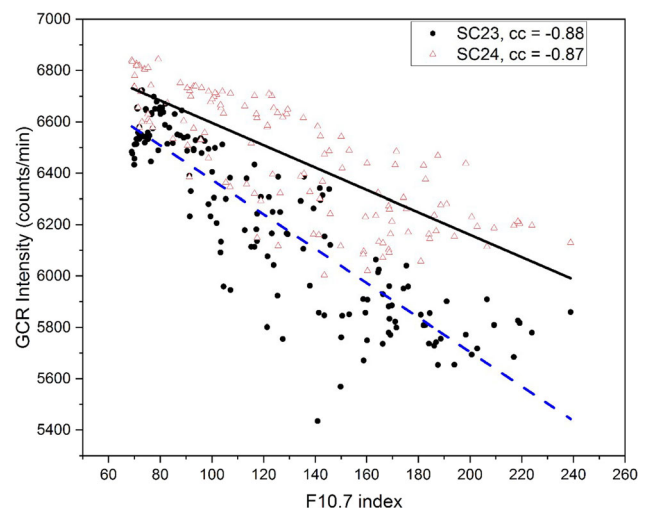
For measuring the temporal variations of solar activity over the solar cycles, the F10.7 cm index is a reliable parameter that appears at the active region at heights where magnetic fields can range from a few hundred to roughly 1500 gauss [24, 25]. The F10.7 index time series behaves similarly to the sunspot number time series (with some differences), including low values of sunspot numbers, which may be zero for monthly averages. In contrast, the smallest values of F10.7 are above 60 solar flux units (SFU), and the sunspot number variation at the high activity phase is more prominent than those at the F10.7 index. $(GCRs)^{-1}$ is displayed as a function of sunspot numbers and the F10.7 index using normalized monthly average values of $(GCRs)^{-1}$, SSN, and F10.7 index. Figure 5 distinctly depicts the $(GCRs)^{-1}$ versus F10.7 line-scatter plot, which is quite similar to the $(GCRs)^{-1}$ versus SSN line-scatter plots.

Figure 5 exhibits the hysteresis phenomena between $(GCRs)^{-1}$ and solar activity tracers, which are referred to as hysteresis plots [26, 27]. Figure 5 shows the hysteresis plots for solar cycles 23 and 24, ascending phase from the beginning to the maximum of each cycle, and descending phase from the maximum to the end of the same cycle. The values for the start of each cycle are shown in the plot's lower-left corner. The values in the upper-right corner are observed around the peak of each cycle. The data points form a trail that evolves in an anti-clockwise manner and closes at the end of the cycle. The plot against $(GCRs)^{-1}$ versus F10.7 behaves similarly to $(GCRs)^{-1}$ versus SSN. The blue and red dotted lines have shown the corresponding normalized values of F10.7 and SSN to the $(GCRs)^{-1}$ at the turning point (maximum). It can be inferred from the plot that the lower value of F10.7 and SSN corresponds to the higher value of $(GCRs)^{-1}$ and vice versa. The hysteresis plots indicate the modulation effects on the GCRs intensity of several events, the function of which fluctuates with the activity cycle. GCRs modulation occurs at various time scales [28, 29], although fluctuations caused by factors beyond the heliosphere can also be included for long-term variations [30]. The cosmic ray flux is also influenced by the local interstellar medium [31, 32], which may not be seen during periods of high solar activity but may become more visible during periods of low solar activity. Figure 6 illustrates a scattered plot of GCRs intensity and F10.7 index; the dashed line shows linear regression between the two variables. GCRs intensity and


Fig. 5 The normalized inverse galactic cosmic ray intensity $(GCRs)^{-1}$ against the normalized fluxes at F10.7 and SSN for cycles 23 and 24. In the main text, we refer to this kind of plot as a hysteresis plot. The blue and red dashed line shows the turning point (maximum) of F10.7 and SSN of both cycles. The curved line shows the ascending and descending phases of the cycles

Fig. 6 Scattered plot between monthly mean GCRs intensity and F10.7 index for solar cycles 23 and 24. The black and blue dashed line shows a linear regression between GCRs and the F10.7 index

F10.7 index have shown strong anticorrelation with each other. In solar cycle 23, Pearson's correlation was found to be $r = -0.88$, and in solar cycle 24, it was $r = -0.87$.

3.2. GCRs intensity vs interplanetary magnetic field (Bz)

Figure 7 presents a scattered plot of GCRs intensity and IMF for solar cycles 23 and 24. From further analysis, we have found that there exists a strong anticorrelation ($r = -0.73$) in solar cycle 23 between these two variables, but in solar cycle 24, a moderate anticorrelation ($r = -0.46$) was observed between them. In solar cycle 24, the anticorrelation of IMF with GCRs intensity was very commendable; this might be due to weak solar activity during the cycle. The more significant fluctuation and time lag can also be seen in IMF (Bz) w.r.t (GCRs intensity)$^{-1}$ in solar cycle 24 compared with solar cycle 23 (Fig. 11).

Cosmic ray intensities are generally known to be inversely linked to Bz [33, 34]. Based on the neutron monitor data analyzed for the period 2006–2009, a strong inverse relationship was established between GCRs intensity and the monthly averaged data of the interplanetary magnetic field strength Bz [35]. The parallel diffusion coefficient ($K_{\parallel}$) is believed to be proportional to 1/B in the theoretical modeling of cosmic rays in the heliosphere [36, 37]. It is commonly assumed that the diffusion coefficient perpendicular to the magnetic field ($K_{\perp}$) scales as the parallel diffusion coefficient [38]. Furthermore, it was proposed that the drift velocities of GCRs increase as Bz decreases [39]. GCRs intensity and interplanetary magnetic field were anticorrelated with each other.
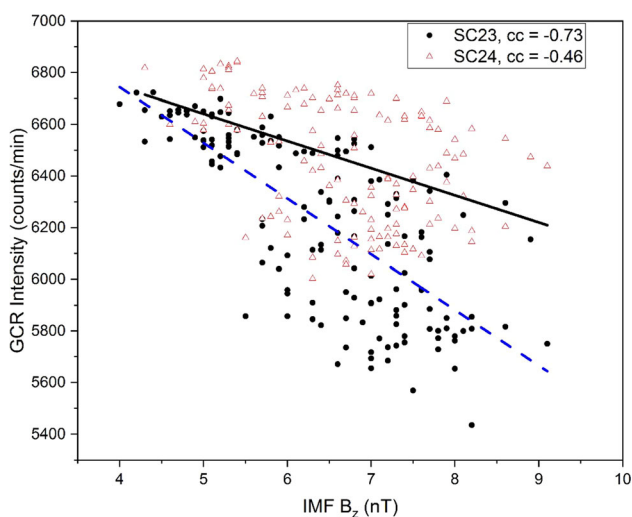
3.3. GCRs intensity vs HCS

The polarity reversal in the heliospheric current sheet occurs roughly in the middle of the solar cycle. The temporal fluctuation of the HCS tilt angle is depicted in Fig. 1. The tilt angle continued to fall after 2014, reaching a minimum of 2.1° in April 2020, which is 22% lower than the solar minimum P22/23 and 53% lower than the solar minimum P23/24. This shallow tilt angle indicates a very tight alignment to the solar equatorial HCS, resulting in increased outward drift velocity (for A > 0) and significantly increased GCRs intensity. Figure 8 shows a scattered plot of GCRs intensity and HCS tilt angle for solar cycles 23 and 24. Figure 8 also reveals that there exists a strong anticorrelation ($r = -0.77$) in solar cycle 23 and ($r = -0.87$) in solar cycle 24.

As cosmic ray particles enter the heliosphere, their strength is modified as they pass through the heliospheric magnetic field embedded in the solar wind [40–42]. The large-scale IMF is made up of the Parker spiral, and thin HCS separates the opposing magnetic hemispheres. Around the maximum of solar activity, the polarity of the solar polar magnetic fields and the heliosphere shifts [43]. Positively modified GCRs particles, i.e., polarity (A > 0, near the equator), flow inward via the poles and subsequently downward from the poles towards the HCS in this arrangement. GCRs particles move inward along the HCS and then upward toward the poles in the opposite polarity configuration (where the field is directed inward in the northern hemisphere and outward in the southern heliosphere), as in solar cycle 23 (1996–2008), referred to as A < 0. As a result, drift effects differentially influence the
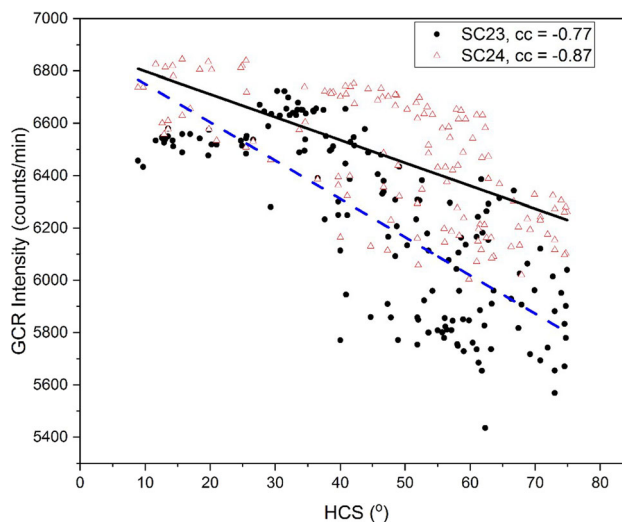

Fig. 7 Scattered plot between monthly mean GCRs intensity and IMF (Bz) for solar cycles 23 and 24. The black and blue dashed line shows a linear regression between GCRs and IMF (Bz)

Fig. 8 Scattered plot between monthly mean GCRs intensity and heliospheric current sheet (HCS) tilt angle for solar cycles 23 and 24. The black and blue dashed line shows a linear regression between GCRs and HCS

entering GCRs particles in the two magnetic configurations A > 0 and A < 0. According to [44], the development of the tilt angle appears systematically different in even- and odd-numbered cycles. Many researchers have studied the temporal variation of GCRs intensity and HCS tilt angle, and these are found to be anticorrelated with each other [45, 46].

3.4. GCRs intensity vs solar wind speed (SWS)

Earlier, Fig. 1 presents the temporal variation of solar wind speed (km s^{-1}) and flow pressure (nPa) for solar cycles 23 and 24. The average SW speed during these two solar cycles was 442 ± 26 and 414 ± 24 km s^{-1}, and the corresponding flow pressure was 2.4 ± 0.2 and 1.8 ± 0.1 nPa, respectively. It has been observed that in the solar minimum 23/24, the SW speed and dynamic pressure were at their lowest levels in the solar minima, which was probably a contributing factor to the abnormally high GCRs intensities in late 2009 [47–49]. Figure 9 depicts the fluctuations in GCRs intensity, solar wind speed, and flow pressure throughout solar cycles 23 and 24. The graph has revealed that at the solar minimum of the 23/24 cycle, the slope of GCRs intensity increased, but the solar wind speed and flow pressure declined rapidly. This has confirmed the anticorrelation of the solar wind speed and flow pressure with the GCRs intensity [48].

4. Time-lag correlative analysis of GCRs intensity with solar and interplanetary parameters

In order to study the temporal delay between GCRs modulation and solar parameters, a time-lag cross-correlation

analysis was performed between monthly mean GCRs intensity and monthly mean SSN, F 10.7 index, HCS, IMF, and SWS, following the technique of [48]. We employed a T-width temporal window centered on a time t, moving within the range $t - T/2$ to $t + T/2$. $T = 50$ months was chosen in this case. Within this interval, the window was adjusted in $\Delta t = 1$- month steps, and Spearman's rank correlation coefficient [ρ] between GCRs intensity and SSN was obtained for each step. The lag between GCRs and SSN was then determined by identifying the maximum correlation coefficient within the period T.

Figure 10 depicts the time lag corresponding to the maximal anti-cross-correlation between monthly averaged GCRs intensity and solar and interplanetary parameters for solar cycles 23 and 24. Table 1 shows the time lag and peak variation in Spearman's correlation coefficient [ρ] and Pearson's correlation coefficient (r) for GCRs intensity versus solar and interplanetary parameters, and the results indicated a substantial agreement between [49] and [50]'s earlier work, giving more evidence on the differentiation between odd and even solar cycles owing to particle transport in the heliosphere.

Solar cycle 24 appears to follow a pattern of nearly no lag for even cycles for GCRs versus SSN, although it does exhibit a lag more significant than that found in prior even cycles [9]. The longer time lag in cycle 24 compared to the previous two even-numbered cycles is most likely due to the profound and extended minimum between Solar Cycles 23 and 24, which delayed the decline in GCRs intensity and resulted in high GCRs intensities [51], as well as the small amplitude of the cycle 24 maximum [52]. The cross-correlation and time lag between the GCRs intensity and interplanetary parameters are presented in Fig. 11. The graph indicated that in solar cycle 23, the IMF has no time

Fig. 9 Temporal variations of solar wind speed (km s^{-1}), flow pressure (nPa), and GCRs intensity (counts/min) for solar cycles 23 and 24. The vertical dashed line shows the extended minimum between the cycles
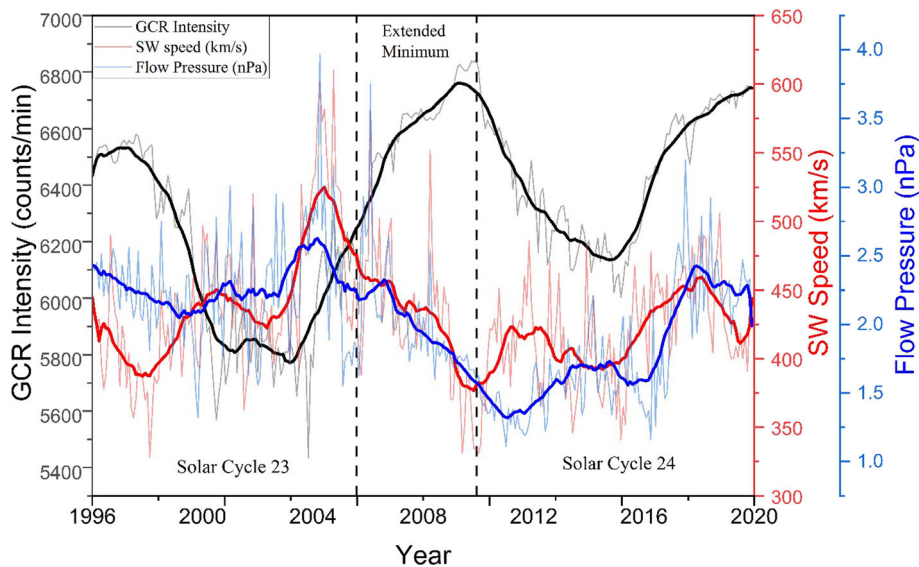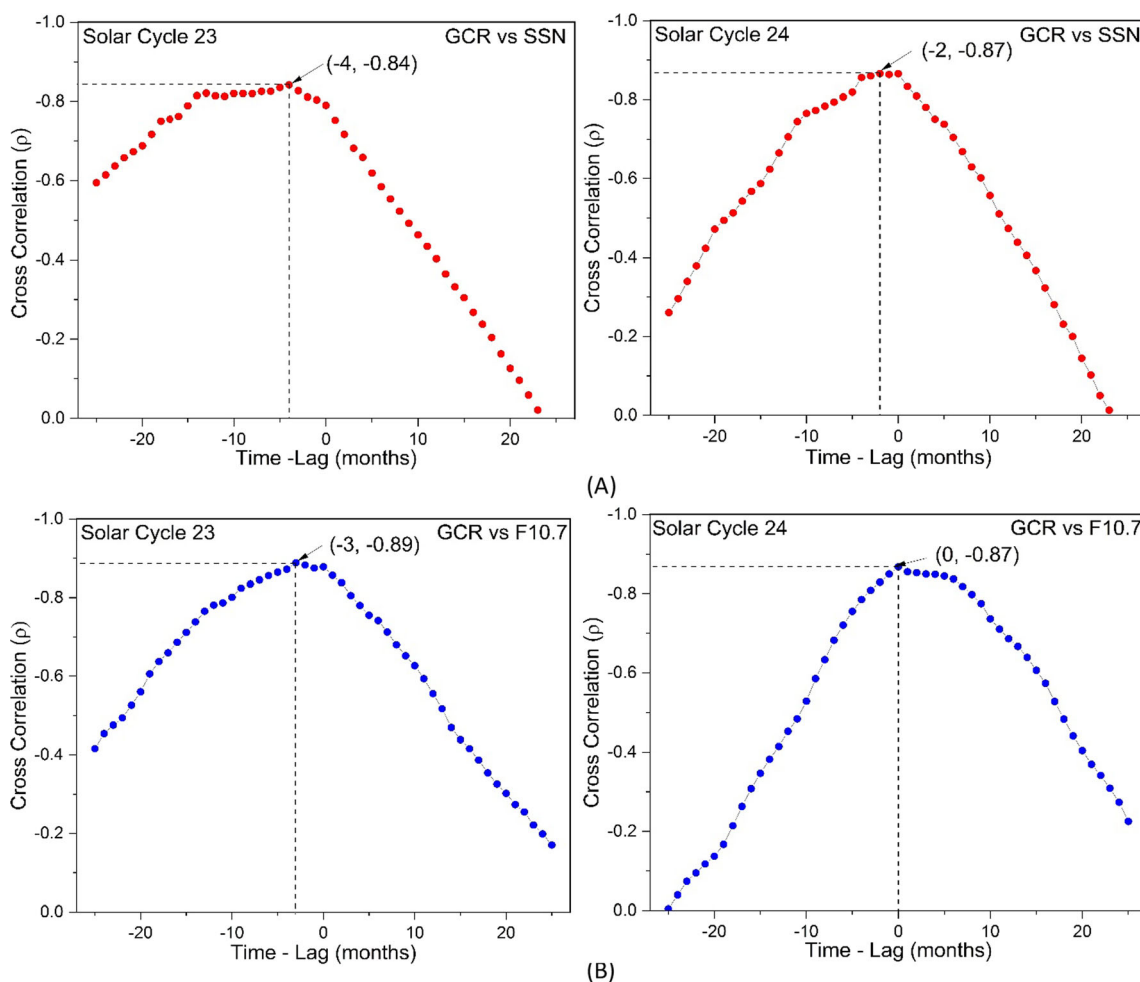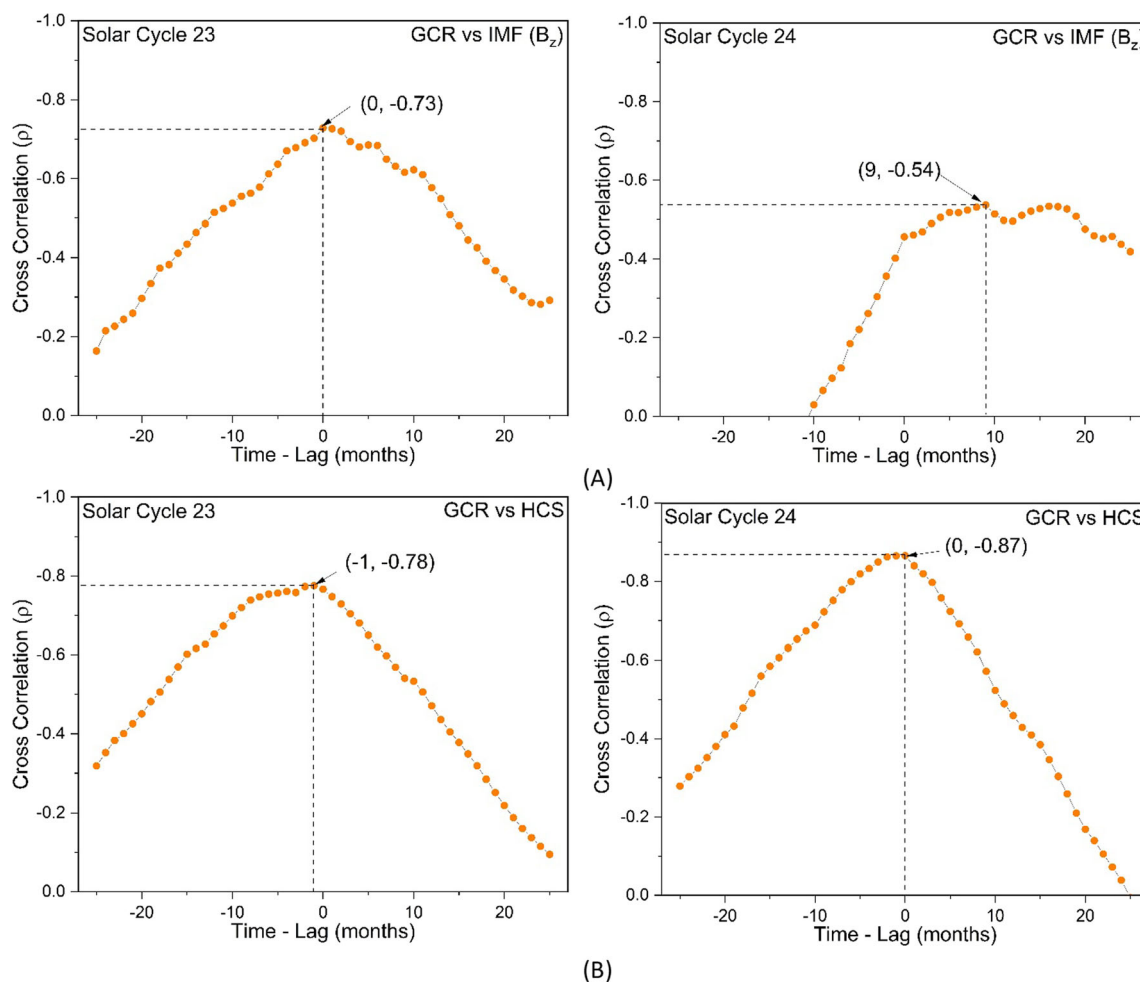
Fig. 10 Variation in the correlation coefficient [ρ] with a time lag between NM GCRs intensity and solar parameters during solar cycles 23 and 24. The vertical and horizontal dashed lines show the time lag in months corresponding to the correlation coefficient

lag. However, in solar cycle 24, there is a 9-month time lag, demonstrating the ineffectiveness of GCRs on the vertical component of the interplanetary magnetic field. The reasons behind these differences are complex, but there are some potential explanations:

- When compared to solar cycle 24, solar cycle 23 was a comparatively robust solar cycle, with more vigorous solar activity and a more significant number of sunspots. During solar cycle 23, more solar activity and a better organized solar magnetic field may have had a more immediate and direct influence on the IMF, resulting in a reduced or nonexistent temporal lag between GCR strength and IMF changes.
- The IMF is carried by the solar wind, which changes in speed, density, and direction. Variability in the solar wind can cause temporal gaps between changes in solar activity and the arrival of solar wind disturbances on Earth, which can influence the observed link between GCR intensity and the IMF.

- Overall heliosphere circumstances, such as the occurrence of coronal mass ejections (CMEs) and other solar events, impact GCR propagation and IMF behavior. Different solar cycle features may cause varied amounts of heliospheric turbulence and complexity, contributing to temporal delays in the GCR-IMF interaction.

Observations during solar cycle 23, which lasted from around 1996 to 2008, revealed a one-month temporal lag in some solar or interplanetary characteristics. This indicates that changes in these characteristics were identified one month before changes in the HCS's orientation or behavior. However, no temporal lag was seen between the HCS and the same solar or interplanetary characteristics during solar cycle 24, which lasted from about 2008 to 2019. Changes in the orientation or dynamics of the HCS appeared to occur concurrently or with minimal delay in this cycle compared to fluctuations in these parameters.

Fig. 11 Variation in the correlation coefficient [ρ] with a time lag between NM GCRs intensity and interplanetary parameters during solar cycles 23 and 24. The vertical and horizontal dashed lines show the time lag in months corresponding to the correlation coefficient

5. Conclusions

As part of this work, we have studied the temporal variations of GCRs intensity and tried analyzing its correlation with solar (SSN, F10.7 index) and interplanetary (Bz, HCS, SWS) parameters during solar cycles 23 (A < 0) and 24 (A > 0) observed during the period 1996–2019. We have collated various aspects and dependencies of GCRs intensity with solar and interplanetary parameters. We have detected a steadily shifting SSN and IMF, approaching lower values at the end of solar cycle 24. In terms of solar wind speed, while it has reached a low point in solar cycle 24 compared to solar cycle 23, its decrease toward the minimum is not identical to that of SSN and Bz. The tilt of the HCS decreased steadily until the end of the minimum when it began to diminish fast to a value that was still more than the smallest tilt angle during the prior minima. However, GCRs intensity has attained a more significant count rate in SC24 compared to SC23.

The increase/decrease in solar wind speed during solar cycle 24 was less than that in the solar cycle 23. After the maximum value obtained in the SWS near the end of solar cycle 23, there was an observed decrease. The decline of the interplanetary magnetic field Bz corresponds to the declining phase of solar activity (SSN, F10.7 index) during solar cycles 23 and 24. Pearson's correlation coefficient (r) for linear regression and Spearman's correlation rank [ρ] for the monotonic dependency of GCRs intensity with solar parameters was strongly anticorrelated in both cycles (Table 1). Pearson's correlation coefficient of GCRs intensity with interplanetary parameters was also strongly anticorrelated in both cycles except for IMF(Bz) versus GCRs intensity in solar cycle 24 (Table 1). The time lag in solar cycle 24 was substantially less compared to solar cycle 23 for solar parameters. However, for interplanetary parameters, there was no lag in both cycles except for IMF in solar cycle 24, which showed a lag of 9 months. The classic model of diffusion, convection, and the adiabatic slowdown effect is used to describe the solar modulation of

GCRs, in which the IMF lines and associated drift processes govern the route of individual particles through the heliosphere. Because of the multiple solar polarity states, this causes distinct variances across nearby solar cycles. As the IMF strength increases, the transport route and diffusion coefficient decrease, increasing GCRs modulation.

Declarations

Conflict of interest Authors declare that they have no conflicts of interest.

References

[1] D Siingh, R P Singh, A K Singhm, M N Kulkarni, A S Gautam and A K Singh *Surv. Geophys.* **32** 659 (2011)

[2] I G Usoskin *Living Rev. Sol. Phys.* **14** 3 (2017)

[3] A Bhargawa and A K Singh *Adv. Space Res.* **68** 2643 (2021)

[4] E Paouris, H Mavromichalaki, A Belov, R Gushchina and V Yanke *Sol. Phys.* **280** 255 (2012)

[5] K Alanko-Huotari, K Mursula, I G Usoskin and G A Kovaltsov *Sol. Phys.* **238** 391 (2006)

[6] J R Jokipii and B T Thomas *Astrophys. J.* **243** 1115 (1981)

[7] M S Potgieter and H Moraal *Astophys. J.* **294** 425 (1985)

[8] M Singh, Y P Singh and Badruddin *J. Atmos. Solar Terr. Phys.* **70** 169 (2008)

[9] E Ross and W J Chaplin *Sol. Phys.* **294** 8 (2019)

[10] S Fu, X Zhang, L Zhao and Y Li *Astrophys. J.* **254** 37 (2021)

[11] S Forbush *J. Geophys. Res.* **59** 525 (1954)

[12] P Väisänen, I G Usoskin and K Mursula *J. Geophys. Res. Space Phys.* **124** 804 (2019)

[13] M S Potgieter *Space Sci. Rev.* **83** 147 (1998)

[14] A Belov *Space Sci. Rev.* **93** 79 (2000)

[15] P Srivastava and A K Singh *J. Emerg. Technol. Innov. Res.* **8** b123 (2021)

[16] J T Hoeksema *Space Sci. Rev.* **72** 137 (1995)

[17] F B McDonald, W R Webber and D V Reames *Geophys. Res. Lett.* **37** L18101 (2010)

[18] J S Rankin, V Bindi, A M Bykov, A C Cummings, S Della Torre, V Florinski, B Heber, M S Potgieter, E C Stone and M Zhang *Space Sci. Rev.* **218** 42 (2022)

[19] M S Potgieter, R A Burger and S E S Ferreira *Space Sci. Rev.* **97** 295 (2001)

[20] A K Singh, D Siingh and R P Singh *Atmos. Environ.* **45** 3806 (2011)

[21] A K Singh and A Tonk *Astrophys. Space Sci.* **353** 367 (2014)

[22] J A Lockwood and W R Webber *J. Geophys. Res.* **84** 120–371 (1979)

[23] J R Jokipii, E H Levy and W B Hubbard *Astrophys. J.* **213** 861 (1977)

[24] S B Akhmedov and G B Gelfreikh *Phys.* **79** 41 (1982)

[25] M J Aschwanden Physics of the Solar Corona. An Introduction with Problems and Solutions 2nd edn. (Berlin: Springer-Verlag) (2005)

[26] K T Bachmann and O R White *Sol. Phys.* **150** 347 (1994)

[27] V K Mishra and A P Mishra *Sol. Phys.* **293** 141 (2018)

[28] M S Potgieter *J. Atmos. Solar Terr. Phys.* **70** 207 (2008)

[29] I G Usoskin, G A Kovaltsov, H Kananen, K Mursala and P Tanskanen Proc. 25th ICRC Durban South Africa **2** p 201 (1997)

[30] K Scherer, H Fichtner, T Borrmann, J Beer, L Desorgher, E Flükiger, H J Fahr, S E Ferreira, U W Langner, M S Potgieter and B Heber *Space Sci. Rev.* **127** 327 (2006)

[31] A Yeghikyan and H Fahr *Astron. Astrophys.* **415** 763 (2004)

[32] I G Usoskin and K Alanko-Yuotari *J. Geophys. Res.* **110** A12108 (2005)

[33] L F Burlaga and N F Ness *J. Geophys. Res.* **103** 29719 (1998)

[34] H V Cane and G Wibberenz *Geophys. Res. Lett.* **26** 56 (1999)

[35] H S Ahluwalia and R C Ygbuhay *Twelfth International Solar Wind Conference* AIP Conf. Proc. **1216** (eds.) M Maksimovic, K Issautier, N Meyer-Vernet, M Moncuquet and F Pantellini p 699 (2010)

[36] J R Jokipii and J M Davila *Astrophys. J.* **248** 1156 (1981)

[37] J P L Reinecke, H Moraal and F B McDonald *J. Geophys. Res.* **105** 12651 (2000)

[38] S E S Ferreira and M S Potgieter *Astrophys. J.* **603** 744 (2004)

[39] R A Mewaldt, A J Davis, K A Lave, R A Leske, E C Stone, M E Wiedenbeck, W R Binns, E R Christian, A C Cummings, G A de Nolfo and M H Israel *Astrophys. J. Lett.* **723** L1 (2010)

[40] E N Parker *Planet Space Sci.* **13** 9 (1965)

[41] U R Rao *Space Sci. Rev.* **12** 719 (1972)

[42] D Venkatesan and Badruddin *Space Sci. Rev.* **52** 121 (1990)

[43] P Janardhan, K Fujiki, M Ingale, S K Bisoi and D Rout *Astron. Astrophys.* **618** A148 (2018)

[44] E W Cliver, I G Richardson and A G Ling *Space Sci. Rev.* **176** 3 (2013)

[45] L Svaalgard and J M Wilcox *Science* **186** 51 (1974)

[46] E J Smith *The Heliospheric Current Sheet and Galactic Cosmic Rays* AIP Conf. Proc. **858** p 104 (2006)

[47] L L Zhao, G Qin, M Zhang and B Heber *J. Geophys. Res. Space Phys.* **119** 1493 (2014)

[48] G D Ihongo and C H T Wang *Astrophys. Space Sci.* **361** 44 (2016)

[49] R A Leske, A C Cummings, R A Mewaldt and E C Stone *Space Sci. Rev.* **176** 253 (2013)

[50] I G Usoskin, H Kananen, K Mursula, P Tanskanen and G A Kovaltsov *J. Geophys. Res.* **103** 9567 (1998)

[51] R P Kane *Sol. Phys.* **289** 2727 (2014)

[52] E Paouris, H Mavromichalaki, A Belov, E Eroshenko and R Gushchina *J. Phys. Conf. Ser.* **632** 012074 (2015)